
Autonomous Behavior and Whole-Brain Dynamics Emerge in Embodied Zebrafish Agents with Model-based Intrinsic Motivation

Reece Keller^{1,2,*} Alyn Tornell² Felix Pei² Xaq Pitkow^{1,3}
Leo Kozachkov^{4,†} Aran Nayebi^{3,1,2,†}

¹Neuroscience Institute, Carnegie Mellon University

²Robotics Institute, Carnegie Mellon University

³Machine Learning Department, Carnegie Mellon University

⁴IBM Thomas J. Watson Research Center, IBM Research

{rdkeller, fcpei, akirsch, xpitkow, anayebi}@andrew.cmu.edu
leokoz8@gmail.com

Abstract

Autonomy is a hallmark of animal intelligence, enabling adaptive and intelligent behavior in complex environments without relying on external reward or task structure. Existing reinforcement learning approaches to exploration in sparse reward and reward-free environments, including class of methods known as *intrinsic motivation*, exhibit inconsistent exploration patterns and thus fail to produce robust autonomous behaviors observed in animals. Moreover, systems neuroscience has largely overlooked the neural basis of autonomy, focusing instead on experimental paradigms where animals are motivated by external reward rather than engaging in unconstrained, naturalistic and task-independent behavior. To bridge these gaps, we introduce a novel model-based intrinsic drive explicitly designed to capture robust autonomous exploration observed in animals. Our method (3M-Progress) motivates naturalistic behavior by tracking divergence between the agent’s current world model and an ethological prior. We demonstrate that artificial embodied agents trained with 3M-Progress capture the explainable variance in behavioral patterns and whole-brain neural-glial dynamics recorded from autonomously-behaving larval zebrafish, introducing the first goal-driven, population-level model of neural-glial computation. Our findings establish a computational framework connecting model-based intrinsic motivation to naturalistic behavior, providing a foundation for building artificial agents with animal-like autonomy.

1 Introduction

Animals exhibit remarkable autonomy, navigating complex environments through self-directed, internally driven behaviors rather than solely responding to external rewards or immediate physiological needs. Unlike typical artificial agents designed to optimize explicit, predefined task objectives in well-defined problem settings, animals intrinsically explore and adapt in open-ended, naturalistic environments where goals are neither clear nor stable. This capacity for autonomous behavior allows organisms, including humans, to flexibly engage in abstract thinking, exploratory learning, and innovative problem-solving. Central to this autonomy is the ability to generate intrinsic goals, seek novel experiences, and continuously refine internal models of the world that inform future actions.

*Corresponding author.

†These authors jointly supervised this work.



Figure 1: Simulation of zebrafish embodiment in varied virtual environments. A) The base 6-link swimmer [1] in a virtual environment with passive fluid force. B) The agent controls the torque exerted by motors at each joint (5 total degrees of freedom) to swim and navigate its environment. C) A custom cosmetic skin to mimic the appearance of larval zebrafish. D) Custom virtual environment to match the experimental parameters of the open loop protocol Mu et al. [2]. The root joint located at the head is fixed during training.

Understanding the interplay between extrinsic and intrinsic motivations remains a fundamental challenge in both systems neuroscience and artificial intelligence, particularly for building robust agents capable of sustained autonomy.

However, current intrinsic motivation methods for exploration in reinforcement learning (RL)—such as curiosity-driven exploration [3–6]—often exhibit fragile and inconsistent behavioral patterns due to difficulties distinguishing between controllable and uncontrollable stimuli, coping with non-stationary environments, and avoiding the “white noise problem” [7]. For example, agents driven by prediction-error alone gets locked into exploring inherently unpredictable or irrelevant aspects of the environment, hindering their ability to develop robust exploratory behaviors [3]. Moreover, existing methods typically fail to produce structured and stable behavioral transitions that characterize genuine autonomous behaviors observed in animals and children [8].

At the same time, systems neuroscience has historically overlooked the cellular basis of autonomy, favoring experimental paradigms centered on explicit external rewards to motivate task-dependent behaviors rather than free, unconstrained exploration. As a result, the cellular mechanisms underlying naturalistic autonomy—particularly those involving whole-brain interactions—remain poorly understood. However, growing experimental, computational, and theoretical evidence suggests that non-neuronal cells, especially astrocytes, play a critical role in the generation of intelligent behavior [2, 9–14]. Owing to their close association with neurons, distinctive connectivity (with a single astrocyte capable of interfacing with up to a million nearby synapses), and ability to perform integrative computations using a hierarchy of timescales, astrocytes are well-positioned to support adaptive, naturalistic, goal-directed behavior [15–20].

To investigate this question, we study autonomy in larval zebrafish—a uniquely valuable animal model due to their optical transparency, which affords whole-brain calcium imaging via light-sheet microscopy [21]. Given that the cellular basis of autonomous behavior remains largely unknown, whole-brain imaging allows us to search across the entire recorded population of approximately 300,000 cells (including 130,000 neurons and 130,000 astrocytes) in aligning our model with brain activity [2]³. We examine a particular cognitive behavior known as futility-induced passivity, observed across the entire animal spectrum [22, 23, 2, 24]. In zebrafish, futility-induced passivity occurs when their active swimming efforts in virtual arenas fail to simulate optic flow. Mu et al. [2] offers rigorous experimental evidence suggesting this transition to passivity is driven neuronal-glia interactions in the lateral medulla oblongata (L-MO) that detect and accumulate sensorimotor feedback error. Noradrenergic (NE) neurons signal swim failures which slowly activate radial astrocyte with extending processes to the NE cluster of L-MO. At a critical level of intracellular calcium, astrocyte processes downstream of L-MO activate GABAergic neurons that suppress swimming. By extensive glia manipulation experiments, Mu et al. [2] demonstrate astrocytes are causally required for reliable futility-induced passivity across animal subjects, underscoring the essential role of astrocytes in neural computation and behavioral state modulation.

In this work, we address the challenge of linking neural-glia computations to the robust autonomous behavior observed in embodied settings by introducing a novel intrinsic reinforcement learning

³The dataset we use is open-source and freely available here.

method termed Model-Memory-Mismatch Progress (3M-Progress). Our approach leverages an internal model that continually compares an agent’s online memory formed by current sensory experience against an ethologically relevant prior memory; intrinsic reward then reinforces transitions between behaviors that where mismatch between memories is maximized relative to its temporal history. 3M-Progress is uniquely capable of producing stable, ethologically-relevant behavioral transitions among several standard intrinsic motivation methods in reinforcement learning.

By training embodied agents with 3M-Progress, we successfully replicate both the robust behavioral transitions observed in autonomously-behaving zebrafish and whole-brain neural-glia dynamics associated with futility-induced passivity. Our agent captures nearly all of the variance in neural and astrocytic activity, marking the first predictive and normative computational model of neural-glia interactions driven by intrinsic motivation.

2 Related Work

Neural-Glia Models Although glial cells—especially astrocytes—are increasingly recognized as crucial to adaptive brain function [2, 9, 17, 14, 19, 20, 11, 25, 26], computational models of neural-glia interactions remain underdeveloped [27]. Existing models of neuron-astrocyte dynamics typically fall into two categories: phenomenological models that reproduce specific experimental findings like calcium oscillations or epileptic activity [28–31], and simplified, “bottom-up” mathematical models that explore theoretical principles based on astrocytes’ unique morphology and anatomy [32–35, 12, 13]. While important, these models are not directly applicable to our setting because they are (a) not yet directly trained on ethological tasks, embodied, or quantitatively validated against real brain data, and (b) typically focused on a single astrocyte, rather than a population of astrocytes. In contrast, we adopt a “top-down” approach: we train a general-purpose recurrent architecture to control an embodied agent to perform ethologically-relevant tasks and find that this imposes strong constraints on the learned representation, allowing us to identify units whose activity patterns closely match those observed in the neurons and astrocytes of larval zebrafish.

Curiosity-driven Exploration Existing methods for curiosity-driven exploration have primarily been evaluated in constrained environments with either handcrafted object-centric inputs [6], or externally-defined rewards such as Atari games (e.g., Random Network Distillation (RND) [4], Intrinsic Curiosity Module (ICM) [3], or Disagreement-based methods [5]) or non-embodied settings like reinforcement learning from human feedback (RLHF) with language agents [36]. While some recent works, such as LEXA [37] or Dreamer [38, 39], extend intrinsic curiosity to robotic control tasks using visual inputs, these methods still focus on exploration relative to extrinsic task-defined rewards. In contrast, our study investigates completely open-ended autonomous behavior, explicitly lacking any extrinsic rewards. Furthermore, unlike prior intrinsic motivation methods that often operate on low-dimensional or handcrafted state representations, our approach is trained end-to-end directly from high-dimensional, biologically realistic sensory streams, providing an ethologically relevant exploration setting more akin to that experienced by biological organisms.

Embodied AI in Neuroscience In the past few years, several works have recently leveraged embodied AI to bridge computational models with neuroscience. Examples include virtual animal models such as Merel et al.’s virtual rodent [40, 41], which facilitates grounded studies of motor control by replicating rodent motor behaviors across various tasks; Janelia’s biomechanically-detailed virtual fly, capable of diverse realistic locomotion driven by reinforcement learning controllers [42]; and Zador et al.’s Embodied Turing Test position paper [43], which emphasizes developing AI models whose sensorimotor capabilities rival those of their biological counterparts.

Our work extends these directions by providing the first predictive and normative computational formalization of neural-glia interactions within embodied agents, trained explicitly via intrinsically-driven exploration. By leveraging biologically-realistic, open-ended scenarios rather than simplified tasks, our approach yields a naturalistic theory of neural-glia computation, offering insights into evolutionary pressures underlying the detailed heterogeneity observed at level of individual neural and glial cells.

3 Methods

Virtual Zebrafish Environment Animals are physically coupled to the environment through their embodiment; this coupling is often referred to as the sensory-motor or perception-action feedback loop. Physical embodiment imposes strong constraints on both the sensory stream from which an agent learns meaningful representations of the world and the actuation system by which the agent manifests behavior. Following this top-down view of biological systems, we constructed an embodied agent and custom virtual environment in the MuJoCo physics engine [44], specifically designed after the ethology of the zebrafish (Figure 1). Leveraging the procedurally generated n -link swimmer and built-in inertial fluid model from the Deepmind Control Suite (dm-control) [1], we construct an ethological environment (Figure 1A-C) in which the agent can freely behave in the presence of both passive and active fluid currents, similar to the gentle water sources to which zebrafish are native. To evaluate our agent in the futility-induced passivity task, we construct a second environment closely matching the open-loop experimental protocol in Mu et al. [2] (Figure 1D). In this environment, agents passively experience a high-contrast grating moving away from the egocentric point-of-view, which simulates backward motion. In the closed-loop condition, the agent is head-free and can learn a positional-homeostasis policy to counteract the perceived backward flow. In the open-loop condition, the agent is head-fixed and its swim commands produce no movement. The passive speed of the moving grating, its colors, and sizing relative to the zebrafish body were determined from experimental parameters in Mu et al. [2]. These environments provide sensory and actuator configurations that closely match the basic structure of free swimming as well as the head-fixed experimental protocol both during model training and model-brain evaluation, which facilitates realistic and meaningful comparison between artificial and biological agents.

Zebrafish Agent Architecture and Policy Training The zebrafish agent is equipped with a recurrent sensory-cognitive architecture to support perception and action in complex environments. Because the autonomous zebrafish behavior recorded by Mu et al. [2] is primarily driven by visual input, we restrict the sensory stream to a vision encoder operating on images with similar resolution to the visual acuity of zebrafish [45]. Sensory features are used by three distinct cognitive networks with modularized objectives. The core and policy modules are implemented as an actor-critic architecture using Long Short-term Memory (LSTM) networks [46] followed by feedforward decoders trained end-to-end with Proximal Policy Optimization (PPO) [47]. Although PPO is a model-free reinforcement learning algorithm, the intrinsic drive module (IDM) learns a world model through online experience that approximates the world state-action transition dynamics in sensory feature-space (as described below). However, this internal model functions only to generate intrinsic reward and is not used for planning or training the policy.

Model-based Intrinsic Reinforcement Learning In classical reinforcement learning, policies are optimized by mapping a desired behavior to maximizing a reward function [48]. This function is one component of the Markov Decision Process (MDP) that formally specifies a task M as a tuple $(\mathcal{S}, \mathcal{A}, T, p_0, r)$, where \mathcal{S} is the space of environment states, \mathcal{A} is the space of actions, $T : \mathcal{S} \times \mathcal{A} \rightarrow \mathcal{P}(\mathcal{S})$ is the transition dynamics (where $\mathcal{P}(\mathcal{S})$ is the set of probability densities over \mathcal{S}), p_0 is the distribution over initial states, and r is the reward function. Importantly, when reward is defined as part of the task MDP, it is *extrinsic* and provided from the environment. However, learning complex behaviors using extrinsic reward can fail for many real-world behaviors where r is extremely sparse (winning a long-horizon game like Go) or intractable to begin with (intellectual pursuits such as knowledge acquisition) without a powerful exploration mechanism that guides behavior. Model-based intrinsic motivation is a class of such mechanisms that leverage internal world models to convey exploration-relevant information in the form intrinsic reward r_t^i . In the absence of any extrinsic reward r_t^e , policy learning with intrinsic motivation is completely self-supervised. In this work, we consider world models ω that take the form of forward dynamics prediction. Let θ parameterize a neural network and $\omega_\theta : \mathcal{S} \times \mathcal{A} \rightarrow \mathcal{P}(\mathcal{S})$. For simplicity, we assume a fixed variance Gaussian density $\omega_\theta = \mathcal{N}(\phi(\mathbf{s}_{t+1}) | \phi(\mathbf{s}_t), \mathbf{a}_t; \mu_\theta, \sigma I)$.

Our Intrinsic Drive Module (2A) implements four alternative model-based intrinsic motivation methods as alternative objectives. *The Intrinsic Curiosity Module (ICM)* [3] defines intrinsic reward as the Shannon surprise of the forward model, $r_t^i := -\log \omega_\theta(\phi_t^f | \phi_t, \mathbf{a}_t)$. I denotes an augmented inverse feature space that is learned on-top of sensory embeddings from ϕ —ICM trains an additional embedding layer ϕ^f using an inverse dynamics model parameterized by θ_I by optimizing an MSE

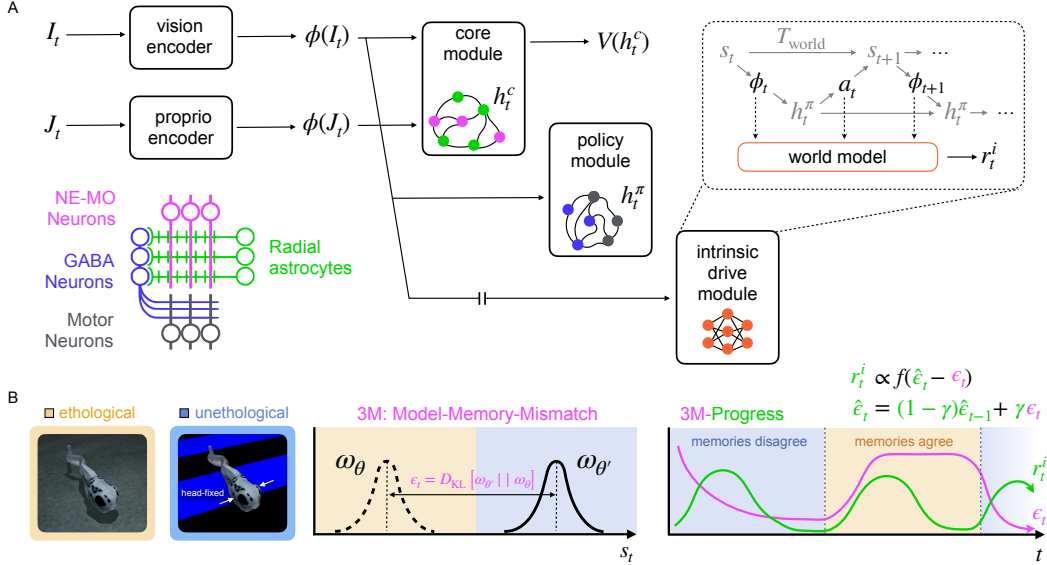


Figure 2: Agent architecture and 3M-Progress. A) Egocentric visual input (I_t) is encoded via a small residual network. Proprioceptive state observations (J_t) are encoded via a small multi-layer perceptron with shortcut paths to both the core and policy module. Sensory features are passed into recurrent LSTM core (h_t^c) and policy (h_t^π) modules that learn a state value function and stochastic policy, respectively. The intrinsic drive module consists of a small multi-layer perceptron that parameterizes a forward dynamics model on sensory features observed from an environment with dynamics T_{world} . B) 3M-Progress uses two memories created from environments with differing transition dynamics. Divergence between the ethological prior ω_θ and the current world-model ω_{θ^r} defines 3M, which is then used as input to leaky integrator \hat{e} to generate intrinsic reward r_t^i .

loss $L(\theta_I) = \mathbb{E}_{\pi_\theta} \|f(\theta_I; \phi_t^I, \phi_{t+1}^I) - \mathbf{a}_t\|_2^2$. *Random Network Distillation (RND)* [4] defines a fixed random nonlinear projection of sensory features $g(\phi)$ and trains a predictor network \hat{g} using an MSE loss $r_t^i := L(\theta_{\text{RND}}) = \mathbb{E}_{\pi_\theta} \|g(\phi_t) - \hat{g}(\theta_{\text{RND}}; \phi_t)\|_2^2$. With the distillation objective as the intrinsic reward, RND does not reinforce behaviors by scoring their predictability by a forward dynamics model as in ICM; instead, the random memory provides a simple exploration bonus for visiting novel states under the policy distribution. *Disagreement* [5] learn an ensemble of world models $\{\omega_{\theta_j}\}_{j=1}^N$ and defines intrinsic reward as $r_t^i := \text{Var}(\{\omega_{\theta_j}\}_{j=1}^N)$ for N randomly initialized world models. Ensemble variances scores the stochasticity of the environment and reinforces state-action pairs for which models disagree. Finally, γ -*Progress* [7] leverages the temporal history of Shannon surprise to define intrinsic reward using prediction gain, $r_t^i := \log \frac{\omega_{\theta_{\text{new}}}}{\omega_{\theta_{\text{old}}}}$, where θ_{new} parameterized a world model after learning on new transitions withheld from an lagging model θ_{old} .

3M-Progress Autonomous animal behavior enables intelligent and robust decision-making in complex environments. Thus, an intrinsic exploration mechanism that captures the ethology of animal autonomy should satisfy at least two desiderata. First, animals do not persevere on random noise or pursue stimuli they cannot causally interact with, so animal autonomy should avoid unpredictable or uncontrollable stimuli. For example, Mu et al. [2] demonstrate that zebrafish transition to passive behavioral states when motor commands elicit unpredictable sensory-feedback (unlearnable) or when sensory-feedback is withheld altogether (uncontrollable). Second, animals exhibit consistent rational decision-making strategies across repeated encounters of the same context, so animal autonomy should converge to reliable and stable behavioral responses in such situations. For example, zebrafish exhibit stable behavioral state-switching in the open-loop experimental protocol across trials and subjects [2]. Existing intrinsic drives that rely on prediction-error alone (ICM, RND) persevere on unlearnable and uncontrollable stimuli by reinforcing stochastic transition dynamics. Learning progress and disagreement overcome this by leveraging temporal dynamics or a world-model ensemble, but together with ICM and RND, suffer from non-stationary rewards—repeated behavioral strategies cause intrinsic reward to saturate such that the reinforcement signal for any single strategy is transient.

Although these properties are suitable for exploration in many robotics and machine learning problem settings [36–39], they may fail to capture the nature of autonomous exploration in animals.

In order to overcome these drawbacks, we introduce Model-Memory-Mismatch Progress (3M-Progress), a novel intrinsic drive that incorporates simple normative qualities of animal autonomy inspired by zebrafish behavior. First, we consider perseveration on unpredictable or uncontrollable stimuli. Learning progress leverages temporal dynamics by comparing predictions from an online memory (θ_{new}) and a long-term memory (θ_{old}), where the memories are mathematically coupled by exponential weight decay. We argue that this long-term memory need not be implemented by decaying the online memory itself—instead, we can decouple these memories completely by learning θ_{old} in a different context and freezing it during learning θ_{new} . Then, the predictions between memories encode a structural bias towards the environment dynamics from the old context, which can then be leveraged to partition the state-action space in the new context into regions where memories systematically agree or systematically disagree.

Formally, let $\omega_{\theta_{old}}(\bar{s}_{t+1} | \bar{s}_t, a_t)$ parameterize a transition density over state-action space $\bar{\mathcal{S}} \times \mathcal{A}$ from an prior MDP context $\mathcal{M} = (\bar{\mathcal{S}}, \mathcal{A}, \bar{T}, \bar{p}_0, \bar{r})$. As $L_{\theta_{old}}$ is minimized, the predicted next state $\mathbb{E}_{\omega_{\theta_{old}}}[\bar{s}_{t+1} | \bar{s}_t, \mathbf{a}]$ approaches the true transition $\bar{s}_{t+1} \sim \bar{T}[\bar{s}_{t+1} | \bar{s}_t, \mathbf{a}_t]$. In the new MDP context \mathcal{M} , the same property holds, where $\mathbb{E}_{\omega_{\theta_{new}}}[\mathbf{s}_{t+1} | \mathbf{s}_t, \mathbf{a}_t] \rightarrow \mathbf{s}_{t+1}$ as $L_{\theta_{new}} \rightarrow 0$. Then, if there exists a state-action pairs $(\bar{s}_t, a_t) \in \bar{\mathcal{S}} \times \mathcal{A}$ and $(\mathbf{s}_t, a_t) \in \mathcal{S} \times \mathcal{A}$ where $\mathcal{D}_{KL}[\bar{T}(\bar{s}_{t+1} | \bar{s}_t, \mathbf{a}_t) || T(\mathbf{s}_{t+1} | \mathbf{s}_t, \mathbf{a}_t)] \approx 0$, then

$$\epsilon_t := \mathcal{D}_{KL}[\omega_{\theta_{old}}(\bar{s}_{t+1} | \bar{s}_t, \mathbf{a}_t) || \omega_{\theta_{new}}(\bar{s}_{t+1} | \bar{s}_t, \mathbf{a}_t)] \propto \|\mu_{\theta_{new}} - \mu_{\theta_{old}}\|_2^2 \approx 0.$$

In other words, state-action pairs with similar environment dynamics result in similar world-model predictions. We term ϵ_t model-memory-mismatch, which loosely partitions the state-action space into model-memory agreement ($\epsilon_t = 0$) and disagreement ($\epsilon_t \gg 0$). Depending on the transition dynamics in each context, model-memory-mismatch encodes distinct behavioral states.

Figure 2B illustrates a specific example inspired by zebrafish, where θ_{old} is learned in an ethological environment—the agent can freely behave and experiences passive fluid forces as it swims and learns to positionally homeostate by resisting an opposing current induced by visual flow. Importantly, the reward in this context is shaped such that the agents rests once it regains its position in order for $\omega_{\theta_{old}}$ to learn a suitable distribution of state-action transitions from both active and passive behaviors. Then, the agent is put into an unethological experimental protocol that headfixes the agent and swim commands do not elicit sensory feedback. As the agent behaves in this environment, it constructs a new memory $\omega_{\theta_{new}}$. The intrinsic reward take a similar mechanistic form as learning progress but filters model-memory-mismatch instead of memory parameters,

$$r_t^i = f(\hat{\epsilon}_t - \epsilon_t),$$

where $\hat{\epsilon}_t = (1 - \gamma)\hat{\epsilon}_{t-1} + \gamma\epsilon_t$ and f is an activation function. Thus, the exponential filter avoids perseveration on behaviors where memories disagree when f is an identity operator. In order to encourage periodic exploration to behavioral partitions where memories disagree, we can simply take f to be any symmetric function. This reinforces deviations from the moving baseline in either direction. Unlike learning progress, this formulation does not saturate as learning unfolds since ϵ_t is computed using a fixed memory. In fact, stable predictions from $\omega_{\theta_{new}}$ due more environment interactions only increases the signal-to-noise ratio in ϵ_t , resulting in more robust behavioral patterns. The shape of f and the progress-horizon γ determine the relative time in each partition and periodicity of switching. In all our experiments, we set $f(x) = |x|$ and $\gamma = 0.99$. Additionally, all experiments include an action penalty $r_t^a = -\lambda\|\mathbf{a}_t\|_2^2$ to encourage exploration of passive behavior during policy learning.

Owing to the formulation of 3M-Progress, learning the state-value function requires, in principle, the presence of units in the core module that are functionally equivalent to neurons in the Noradrenergic cluster of the Medulla Oblongata (NE-MO) and radial astrocytes identified in zebrafish by Mu et al. [2] (2A). 3M-Progress detects sensory-motor mismatch using a prior memory as an *expectation* of how action is coupled to sensory-feedback under normal, ethological environment dynamics (2C). This is functionally equivalent to signaling failed swim-attempts by NE-MO neurons in zebrafish. Such a signal directly implicates a biological prior that encodes how swim-attempts *should* be coupled to visual feedback. Similarly, the exponential weighted average is a discrete-time leaky integrator on model-memory-mismatch (NE-MO input), which is functionally equivalent to radial astrocytes that accumulate NE-MO signals during failed swim-attempts and decay during passivity (2C).

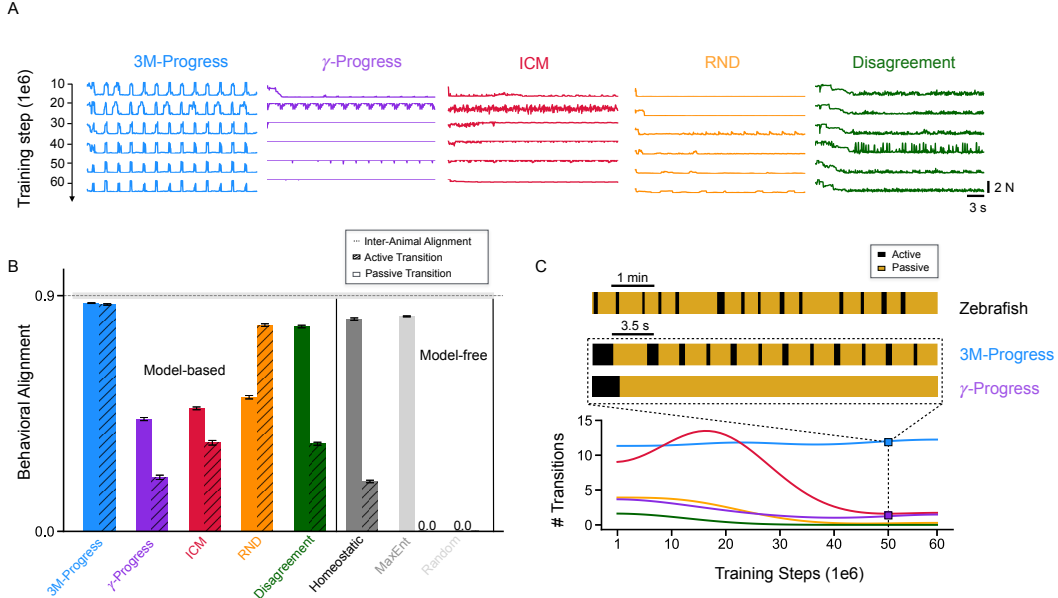


Figure 3: Model-Behavioral Alignment. A) Swim power traces of artificial agents with different intrinsic drives throughout training. B) Pearson’s r correlation between agent swim power (joint torques) and zebrafish swim power (motor neuron activity) for active and passive behavioral transitions. C) (Top) Timecourse of active-passive transitions in zebrafish compared against stationary behavior from progress-driven agents for a single rollout. (Bottom) Average number of behavioral transitions per rollout across training for different intrinsic drives.

3.1 Model-Brain and Inter-Animal Alignment

To rigorously evaluate our embodied agents against whole-brain response patterns collected by [2], neural-glial recordings from zebrafish were first aligned to periods specifically capturing behavioral state transitions between active swimming and futility-induced passivity. Correspondingly, latent states and predicted neural-glial responses from our agents were aligned to these same experimentally defined epochs using event-triggered averaging around transition events. To quantify model-brain alignment, we employed a stringent “One-to-One” mapping, in which each neural or astrocytic unit from the biological data was matched directly to the single most correlated artificial unit from the computational model. Although this mapping is typically too restrictive for capturing inter-animal alignment in heterogeneous neural populations for brain-region-specific (e.g. *not* whole brain) data in other animals (as shown in prior sensory [49] and cognitive systems [50] where full linear regression is necessary), we found it was fully sufficient here, due to the exceptional whole-brain reliability of zebrafish neural-glial responses during futility-induced passivity. Indeed, inter-animal alignment computed from pairwise correlations between individual zebrafish was nearly 100%, establishing a robust empirical ceiling for evaluating model performance.

Specifically, inter-animal alignment was computed as the correlation of neural-glial response patterns across pairs of zebrafish within aligned epochs, thus formally defining the upper bound of predictivity achievable by any candidate model. This approach ensures that successful computational models achieve neural predictivity indistinguishable from biological measurements, within the bounds set by natural biological variability. Together, these procedures allowed us to precisely quantify model-brain alignment, and achieving close correspondence between artificial and biological responses under this strict One-to-One mapping criterion provides strong evidence that our intrinsic motivation-driven embodied agents effectively capture the detailed neural and glial dynamics underlying autonomous behavioral transitions in zebrafish.

3.2 Model-Behavioral Alignment

To quantify similarity between biological zebrafish and our artificial agents, we use Pearson’s r as a metric between the respective swim power readouts for each system surrounding state transitions. In

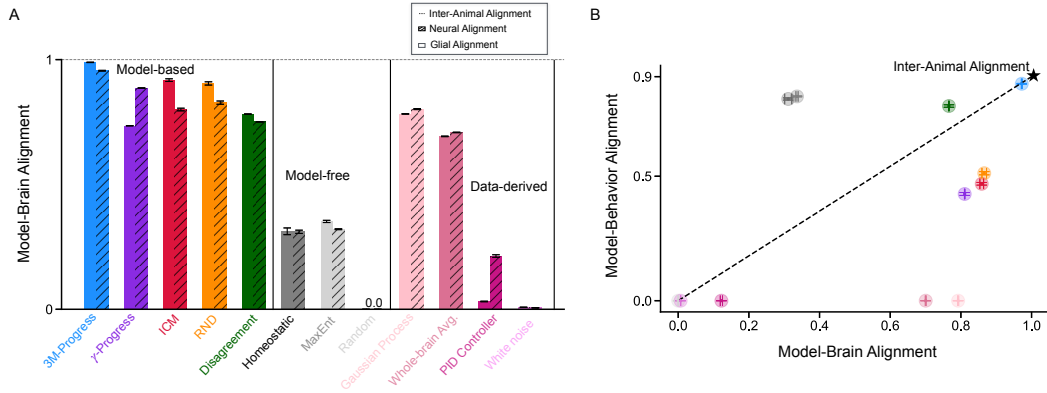


Figure 4: Model-Brain Alignment. A) Noise-corrected Pearson’s r correlation between whole-brain neural and glial units and artificial units from trained agents during passive transitions. B) Model scores on behavioral and whole-brain alignment during passive transitions.

zebrafish, swim power was calculated as the standard deviation over a 10ms window of recorded tail motor nerve signals following Mu et al. [2]. We use the same passive and active transitions windows identified by Mu et al. [2] to compute the inter-animal behavioral alignment across 11 subjects by applying the metric to swim power after smoothing and normalization over a 20 second window surrounding the transition time. For the artificial agents, we take the norm of their joint torques as swim power and identify behavioral transitions as high-frequency changes in swim power above a threshold of 1 Newton. This threshold was determined empirically by recording joint activations during active and passive behaviors in the default swim task in the dm-control suite [1]. Model-behavioral consistency is then computed by applying the metric between segmented zebrafish data and the agent’s swim power surrounding these transitions over a 20-step window.

4 Results

3M-Progress Agents Replicate Behavioral Patterns Observed in Zebrafish We next assessed the ability of intrinsic motivation methods to replicate detailed behavioral patterns observed in biological zebrafish during autonomous exploration. Behavioral alignment was quantified by comparing locomotor trajectories and state transitions (active to passive and back) between artificial agents and zebrafish across multiple trials and subjects. 3M-Progress discovers ethologically-relevant behavioral state transitions by 10 million environment steps, whereas other intrinsic drives display transient strategies and stabilize on complete passivity or activity over training (Figure 3A). Agents trained with 3M-Progress exhibited the highest model-brain alignment, successfully capturing the dynamics of behavioral transitions recorded in the biological data (Figure 3B).

Additionally, agents trained with traditional intrinsic motivation methods such as ICM, RND, Disagreement, and γ -progress showed significantly lower alignment and failed to capture the characteristic stable cycling between activity states (Figure 3B-C).

3M-Progress Agents Saturate Explainable Variance of Whole-Brain Neural-Glial Dynamics

To evaluate how closely intrinsic motivation-driven agents matched zebrafish neural-glial dynamics, we compared model predictions to whole-brain calcium imaging data recorded during futility-induced passivity transitions. Neural-glial alignment was quantified using a One-to-One mapping, where each recorded biological neural or astrocytic unit was matched to the single most correlated artificial unit from the model. Strikingly, 3M-Progress agents captured nearly all of the explaining explainable variance in neural and astrocytic activity, markedly outperforming all existing intrinsic motivation methods, as well as baseline controls (Figure 4A). Model-free intrinsic drive controls include energy cost (homeostatic), entropy bonus (MaxEnt), and a randomly initialized agent. Data-derived controls include a Gaussian Process fit to neural-glial responses, proportional-integral-derivative (PID) control, average neural-glial population response, and white-noise. In fact, the 3M-Progress agent is the only model that is best aligned with *both* the behavioral alignment and neural-glial alignment, highlighting

that accurate behavioral modeling closely corresponds with capturing detailed neural dynamics (Figure 4B), thereby passing the NeuroAI Turing test on this dataset [51].

Latent Dynamics of 3M-Progress Agents Reflect Underlying Neural-Glial Computations

Given that 3M-Progress best matched both behavioral and neural-glial alignment among all candidate models, we then characterized the internal dynamics of the 3M-Progress agent by performing Principal Component Analysis (PCA) on its *in silico* neural-glial population during active-to-passive state transitions. PCA revealed that the dominant latent dimensions of the agent’s core module closely mirrors whole-brain neural-glial dynamics measured from biological zebrafish, whereby glial responses accumulate evidence of motor futility via noradrenergic signaling to drive behavioral suppression, and neural responses reflect transient activation patterns associated with detecting mismatches between expected and actual sensory outcomes during unsuccessful swim attempts. This analysis demonstrates that the 3M-Progress intrinsic motivation mechanism not only generates realistic behavior, but also robustly captures fundamental internal neural-glial computations underlying autonomous exploration and behavioral state transitions (Figure 5).

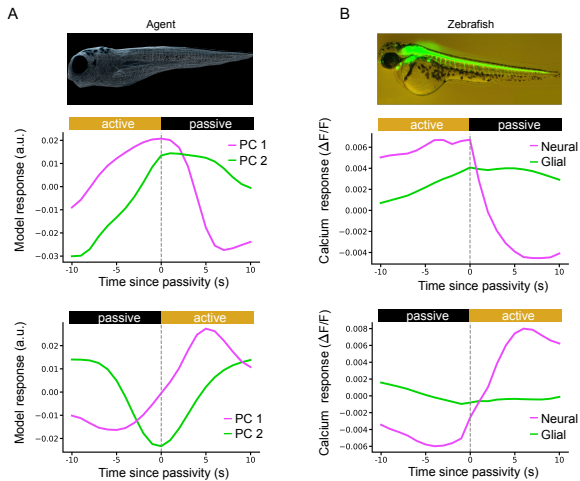


Figure 5: Latent dynamics of 3M-Progress agent’s internal activations compared with whole-brain neural-glial response in zebrafish. A) Principal components during passive and active transitions in the agent. B) Average whole-brain neural-glial response during passive and active transitions in a zebrafish subject.

5 Discussion

We introduced 3M-Progress, a novel intrinsic motivation formulation grounded in continuously tracking divergences between an internal world model and ethologically relevant memory, which robustly produced naturalistic transitions between active and passive behavioral states. Unlike prior intrinsic motivation methods that suffer from behavioral inconsistency and stochasticity, 3M-Progress reliably generated stable cycling behaviors closely matching those observed in biological zebrafish. Our work provides the first goal-driven computational model of neural-glial interactions and demonstrates its ability to replicate both behavioral patterns and underlying neural-glial computation observed during autonomous exploration in larval zebrafish.

Specifically, 3M-Progress agents were uniquely successful in capturing whole-brain neural-glial activity among all candidate models. We showed that artificial agent’s internal latent dynamics mirror neural-glial computation, wherein astrocytic responses accumulate evidence of motor futility through noradrenergic signaling to trigger behavioral suppression, while neural populations transiently encode mismatches between expected and observed sensory outcomes. Thus, our approach provides both behavioral, population-level, and mechanistic alignment with larval zebrafish.

Our findings suggest two complementary evolutionary constraints for developing robust, animal-like autonomous agents: (1) maintaining an intrinsic drive informed by memory, and (2) continuously monitoring divergences between this memory and the predictions of its world model. Functionally, tracking these mismatches within reinforcement learning frameworks allows artificial agents to identify ineffective strategies, update internal models adaptively, and redirect exploration towards more fruitful actions. Such mechanisms offer significant potential for enhancing the robustness and adaptivity of artificial autonomous systems, particularly in open-ended environments lacking clear external reward.

Limitations and Future Work Despite these strengths, several limitations merit consideration. Our current analyses primarily focused on passive behavioral transitions within constrained virtual environments, limiting ecological realism. Future work could extend both the artificial agents’ environments and the neural experiments to richer ecological settings and more complex behavioral repertoires, providing stronger and more diverse constraints on computational models of autonomy. Related to improving the richness of the environment, the biomechanical realism of the body could be further expanded to include muscles, providing additional constraints on the lower-level control problem. Additionally, while our model captures essential neuron-glia interactions at a population level, it abstracts away detailed biochemical signaling mechanisms within astrocytes and neurons. Incorporating more biologically detailed models of these subcellular processes could aid in providing predictions about signaling mechanisms at the subcellular scale. Nevertheless, our current approach provides a robust foundation for systematically investigating these open questions, paving the way for building more sophisticated autonomous artificial agents capable of adaptive exploration and flexible decision-making comparable to biological organisms.

Acknowledgements

We thank Misha Ahrens, Chris Doyle, and Yu Mu for helpful discussions. A.N. was supported in part by a grant from the Burroughs Wellcome Fund. X.P. and R.K. were supported in part by the National Science Foundation and DoD OUSD (R & E) under Cooperative Agreement PHY-2229929 (The NSF AI Institute for Artificial and Natural Intelligence, ARNI).

References

- [1] Yuval Tassa, Yotam Doron, Alistair Muldal, Tom Erez, Yazhe Li, Diego de Las Casas, David Budden, Abbas Abdolmaleki, Josh Merel, Andrew Lefrancq, et al. Deepmind control suite. *arXiv preprint arXiv:1801.00690*, 2018.
- [2] Yu Mu, Davis V Bennett, Mikail Rubinov, Sujatha Narayan, Chao-Tsung Yang, Masashi Tanimoto, Brett D Mensh, Loren L Looger, and Misha B Ahrens. Glia accumulate evidence that actions are futile and suppress unsuccessful behavior. *Cell*, 178(1):27–43, 2019.
- [3] Deepak Pathak, Pulkit Agrawal, Alexei A Efros, and Trevor Darrell. Curiosity-driven exploration by self-supervised prediction. In *International conference on machine learning*, pages 2778–2787. PMLR, 2017.
- [4] Yuri Burda, Harrison Edwards, Amos Storkey, and Oleg Klimov. Exploration by random network distillation. *arXiv preprint arXiv:1810.12894*, 2018.
- [5] Deepak Pathak, Dhiraj Gandhi, and Abhinav Gupta. Self-supervised exploration via disagreement. In *International conference on machine learning*, pages 5062–5071. PMLR, 2019.
- [6] Kuno Kim, Megumi Sano, Julian De Freitas, Nick Haber, and Daniel Yamins. Active world model learning with progress curiosity. In *International conference on machine learning*, pages 5306–5315. PMLR, 2020.
- [7] Jürgen Schmidhuber. Formal theory of creativity, fun, and intrinsic motivation (1990–2010). *IEEE transactions on autonomous mental development*, 2(3):230–247, 2010.
- [8] Nick Haber, Damian Mrowca, Stephanie Wang, Li F Fei-Fei, and Daniel L Yamins. Learning to play with intrinsically-motivated, self-aware agents. *Advances in neural information processing systems*, 31, 2018.
- [9] Jun Nagai, Xinzhu Yu, Thomas Papouin, Eunji Cheong, Marc R Freeman, Kelly R Monk, Michael H Hastings, Philip G Haydon, David Rowitch, Shai Shaham, et al. Behaviorally consequential astrocytic regulation of neural circuits. *Neuron*, 109(4):576–596, 2021.
- [10] Laurie M Robin, José F Oliveira da Cruz, Valentin C Langlais, Mario Martin-Fernandez, Mathilde Metna-Laurent, Arnau Busquets-Garcia, Luigi Bellocchio, Edgar Soria-Gomez, Thomas Papouin, Marjorie Varilh, et al. Astroglial cb1 receptors determine synaptic d-serine availability to enable recognition memory. *Neuron*, 98(5):935–944, 2018.

- [11] Michael R Williamson, Wookbong Kwon, Junsung Woo, Yeunjung Ko, Ehson Maleki, Kwanha Yu, Sanjana Murali, Debosmita Sardar, and Benjamin Deneen. Learning-associated astrocyte ensembles regulate memory recall. *Nature*, pages 1–9, 2024.
- [12] Leo Kozachkov, Ksenia V Kastanenko, and Dmitry Krotov. Building transformers from neurons and astrocytes. *Proceedings of the National Academy of Sciences*, 120(34):e2219150120, 2023.
- [13] Leo Kozachkov, Jean-Jacques Slotine, and Dmitry Krotov. Neuron–astrocyte associative memory. *Proceedings of the National Academy of Sciences*, 122(21):e2417788122, 2025. doi: 10.1073/pnas.2417788122. URL <https://www.pnas.org/doi/abs/10.1073/pnas.2417788122>.
- [14] Ciaran Murphy-Royal, ShiNung Ching, and Thomas Papouin. A conceptual framework for astrocyte function. *Nature Neuroscience*, pages 1–9, 2023.
- [15] Zhiguo Ma, Tobias Stork, Dwight E Bergles, and Marc R Freeman. Neuromodulators signal through astrocytes to alter neural circuit activity and behaviour. *Nature*, 539(7629):428–432, 2016.
- [16] Jillian L Stobart, Kim David Ferrari, Matthew JP Barrett, Chaim Glück, Michael J Stobart, Marc Zuend, and Bruno Weber. Cortical circuit activity evokes rapid astrocyte calcium signals on a similar timescale to neurons. *Neuron*, 98(4):726–735, 2018.
- [17] Adi Doron, Alon Rubin, Aviya Benmelech-Chovav, Netai Benaim, Tom Carmi, Ron Refaeli, Nechama Novick, Tirzah Kreisel, Yaniv Ziv, and Inbal Goshen. Hippocampal astrocytes encode reward location. *Nature*, 609(7928):772–778, 2022.
- [18] Roberta De Ceglia, Ada Ledonne, David Gregory Litvin, Barbara Lykke Lind, Giovanni Carriero, Emanuele Claudio Latagliata, Erika Bindocci, Maria Amalia Di Castro, Iaroslav Savtchouk, Ilaria Vitali, et al. Specialized astrocytes mediate glutamatergic gliotransmission in the cns. *Nature*, 622(7981):120–129, 2023.
- [19] Kyungchul Noh, Woo-Hyun Cho, Byung Hun Lee, Dong Wook Kim, Yoo Sung Kim, Keebum Park, Minkyu Hwang, Ellane Barcelon, Yoon Kyung Cho, C Justin Lee, et al. Cortical astrocytes modulate dominance behavior in male mice by regulating synaptic excitatory and inhibitory balance. *Nature Neuroscience*, 26(9):1541–1554, 2023.
- [20] Peter Rupprecht, Sian N Duss, Denise Becker, Christopher M Lewis, Johannes Bohacek, and Fritjof Helmchen. Centripetal integration of past events in hippocampal astrocytes regulated by locus coeruleus. *Nature Neuroscience*, pages 1–13, 2024.
- [21] Misha B Ahrens, Michael B Orger, Drew N Robson, Jennifer M Li, and Philipp J Keller. Whole-brain functional imaging at cellular resolution using light-sheet microscopy. *Nature methods*, 10(5):413–420, 2013.
- [22] Joseph V Brady, Robert W Porter, Donald G Conrad, and John W Mason. Avoidance behavior and the development of duodenal ulcers. *Journal of the Experimental Analysis of Behavior*, 1(1):69, 1958.
- [23] Robert M Camp and John D Johnson. Repeated stressor exposure enhances contextual fear memory in a beta-adrenergic receptor-dependent process and increases impulsivity in a non-beta receptor-dependent fashion. *Physiology & behavior*, 150:64–68, 2015.
- [24] Natalija Popović, Nicanor Morales-Delgado, Ernesto De la Cruz-Sánchez, and Miroljub Popović. Rats conserve passive avoidance retention level throughout the light phase of diurnal cycle. *Physiology & Behavior*, 268:114234, 2023.
- [25] Cagla Eroglu. Astrocytes, hidden puppet masters of the brain. *Science*, 388(6748):705–706, 2025. doi: 10.1126/science.adx7102. URL <https://www.science.org/doi/abs/10.1126/science.adx7102>.

- [26] Katheryn B. Lefton, Yifan Wu, Yanchao Dai, Takao Okuda, Yufen Zhang, Allen Yen, Gareth M. Rurak, Sarah Walsh, Rachel Manno, Bat-Erdene Myagmar, Joseph D. Dougherty, Vijay K. Samineni, Paul C. Simpson, and Thomas Papouin. Norepinephrine signals through astrocytes to modulate synapses. *Science*, 388(6748):776–783, 2025. doi: 10.1126/science.adq5480. URL <https://www.science.org/doi/abs/10.1126/science.adq5480>.
- [27] Ksenia V Kastanenka, Rubén Moreno-Bote, Maurizio De Pittà, Gertrudis Perea, Abel Erasó-Pichot, Roser Masgrau, Kira E Poskanzer, and Elena Galea. A roadmap to integrate astrocytes into systems neuroscience. *Glia*, 68(1):5–26, 2020.
- [28] Leo Kozachkov and Konstantinos P Michmizos. The causal role of astrocytes in slow-wave rhythmogenesis: A computational modelling study. *arXiv preprint arXiv:1702.03993*, 2017.
- [29] Maurizio De Pittà, Mati Goldberg, Vladislav Volman, Hugues Berry, and Eshel Ben-Jacob. Glutamate regulation of calcium and ip3 oscillating and pulsating dynamics in astrocytes. *Journal of biological physics*, 35(4):383–411, 2009.
- [30] Mati Goldberg, Maurizio De Pittà, Vladislav Volman, Hugues Berry, and Eshel Ben-Jacob. Non-linear gap junctions enable long-distance propagation of pulsating calcium waves in astrocyte networks. *PLoS computational biology*, 6(8):e1000909, 2010.
- [31] Vladislav Volman, Maxim Bazhenov, and Terrence J Sejnowski. Computational models of neuron-astrocyte interaction in epilepsy. *Frontiers in computational neuroscience*, 6:58, 2012.
- [32] Leo Kozachkov and Konstantinos P Michmizos. Sequence learning in associative neuronal-astrocytic networks. In *Brain Informatics: 13th International Conference, BI 2020, Padua, Italy, September 19, 2020, Proceedings 13*, pages 349–360. Springer, 2020.
- [33] Vladimir Ivanov and Konstantinos Michmizos. Increasing liquid state machine performance with edge-of-chaos dynamics organized by astrocyte-modulated plasticity. *Advances in neural information processing systems*, 34:25703–25719, 2021.
- [34] Maurizio De Pittà and Nicolas Brunel. Multiple forms of working memory emerge from synapse–astrocyte interactions in a neuron–glia network model. *Proceedings of the National Academy of Sciences*, 119(43):e2207912119, 2022.
- [35] Lulu Gong, Fabio Pasqualetti, Thomas Papouin, and ShiNung Ching. Astrocytes as a mechanism for meta-plasticity and contextually-guided network function. *arXiv preprint arXiv:2311.03508*, 2023.
- [36] Haoran Sun, Yekun Chai, Shuohuan Wang, Yu Sun, Hua Wu, and Haifeng Wang. Curiosity-driven reinforcement learning from human feedback. *arXiv preprint arXiv:2501.11463*, 2025.
- [37] Russell Mendonca, Oleh Rybkin, Kostas Daniilidis, Danijar Hafner, and Deepak Pathak. Discovering and achieving goals via world models. *Advances in Neural Information Processing Systems*, 34:24379–24391, 2021.
- [38] Danijar Hafner, Timothy Lillicrap, Jimmy Ba, and Mohammad Norouzi. Dream to control: Learning behaviors by latent imagination. *arXiv preprint arXiv:1912.01603*, 2019.
- [39] Danijar Hafner, Jurgis Pasukonis, Jimmy Ba, and Timothy Lillicrap. Mastering diverse control tasks through world models. *Nature*, pages 1–7, 2025.
- [40] Josh Merel*, Diego Aldarondo*, Jesse Marshall*, Yuval Tassa, Greg Wayne, and Bence Ölveczky. Deep neuroethology of a virtual rodent. *International Conference on Learning Representations*, 2020.
- [41] Diego Aldarondo, Josh Merel, Jesse D Marshall, Leonard Hasenclever, Ugne Klibaite, Amanda Gellis, Yuval Tassa, Greg Wayne, Matthew Botvinick, and Bence P Ölveczky. A virtual rodent predicts the structure of neural activity across behaviors. *Nature*, pages 1–3, 2024.
- [42] Roman Vaxenburg, Igor Siwanowicz, Josh Merel, Alice A Robie, Carmen Morrow, Guido Novati, Zinovia Stefanidi, Gert-Jan Both, Gwyneth M Card, Michael B Reiser, et al. Whole-body simulation of realistic fruit fly locomotion with deep reinforcement learning. *bioRxiv*, pages 2024–03, 2024.

- [43] Anthony Zador, Sean Escola, Blake Richards, Bence Ölveczky, Yoshua Bengio, Kwabena Boahen, Matthew Botvinick, Dmitri Chklovskii, Anne Churchland, Claudia Clopath, et al. Catalyzing next-generation artificial intelligence through neuroai. *Nature communications*, 14 (1):1597, 2023.
- [44] Emanuel Todorov, Tom Erez, and Yuval Tassa. Mujoco: A physics engine for model-based control. In *2012 IEEE/RSJ international conference on intelligent robots and systems*, pages 5026–5033. IEEE, 2012.
- [45] Marion F Haug, Oliver Biehler, Kaspar P Mueller, and Stephan CF Neuhaus. Visual acuity in larval zebrafish: behavior and histology. *Frontiers in zoology*, 7:1–7, 2010.
- [46] Sepp Hochreiter and Jürgen Schmidhuber. Long short-term memory. *Neural computation*, 9(8): 1735–1780, 1997.
- [47] John Schulman, Filip Wolski, Prafulla Dhariwal, Alec Radford, and Oleg Klimov. Proximal policy optimization algorithms. *arXiv preprint arXiv:1707.06347*, 2017.
- [48] Richard S Sutton, Andrew G Barto, et al. *Reinforcement learning: An introduction*, volume 1. MIT press Cambridge, 1998.
- [49] Aran Nayebi*, Nathan CL Kong*, Chengxu Zhuang, Justin L Gardner, Anthony M Norcia, and Daniel LK Yamins. Mouse visual cortex as a limited resource system that self-learns an ecologically-general representation. *PLOS Computational Biology*, 19, 2023.
- [50] Aran Nayebi, Alexander Attinger, Malcolm Campbell, Kiah Hardcastle, Isabel Low, Caitlin Mallory, Gabriel Mel, Ben Sorscher, Alex Williams, Surya Ganguli, Lisa M Giocomo, and Daniel LK Yamins. Explaining heterogeneity in medial entorhinal cortex with task-driven neural networks. *Advances in Neural Information Processing Systems*, 34, 2021.
- [51] Jenelle Feather*, Meenakshi Khosla*, N Murty*, and Aran Nayebi*. Brain-model evaluations need the neuroai turing test. *arXiv preprint arXiv:2502.16238*, 2025.
- [52] John Schulman, Philipp Moritz, Sergey Levine, Michael Jordan, and Pieter Abbeel. High-dimensional continuous control using generalized advantage estimation. *arXiv preprint arXiv:1506.02438*, 2015.
- [53] Diederik P Kingma. Adam: A method for stochastic optimization. *arXiv preprint arXiv:1412.6980*, 2014.

Appendix

In the descriptions below, we recycle several symbols between sections. Within sections, symbols are defined and self-consistent, so it should be clear to the reader what we are referring to. All experimental results involving policy rollouts are averaged across 8 random evaluation seeds.

A Model-Brain Alignment for Active Transitions

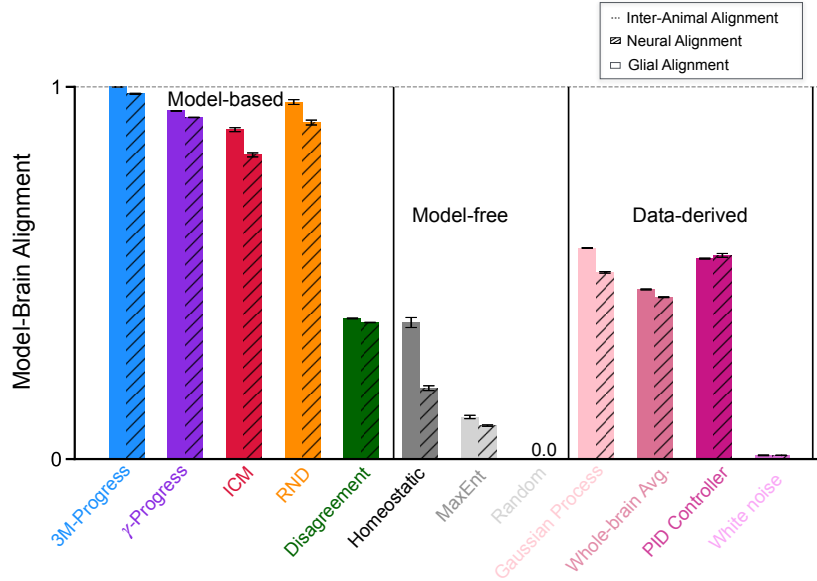


Figure 6: Noise-corrected Pearson’s r correlation between whole-brain neural and glial units and artificial units from trained agents during active transitions.

B Model-Brain Alignment per Agent Module

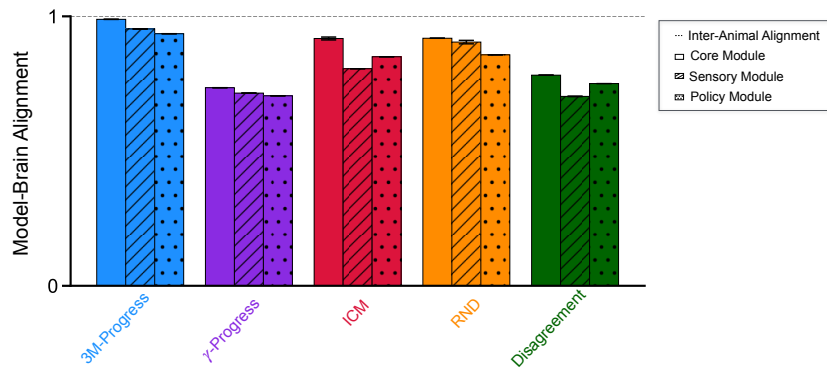


Figure 7: Model-Brain Alignment for Passive Transitions per Module. Core and policy modules include each LSTM block along with hidden layers of their MLP decoders. The sensory module includes the last layer of the proprioceptive and vision encoders.

C Description of Control Models

Homeostatic Agent One straightforward way to achieve a passive behavioral transition is to simply add an action-cost that outweighs any other positive reward signal. In the presence of a fixed or

nonexistent extrinsic reward signal which the agent has no control over (such as in the open-loop protocol), an action-cost encourages the agent to become passive, corresponding to a metabolic constraint or homeostatic regulation of energy. We implement this cost as the magnitude of the force exerted by the agent’s motors, $c(a_t) = \lambda \|\mathbf{a}_t\|_2$. In all our experiments, we set $\lambda = 1$.

Maximum Entropy (MaxEnt) Agent Maximum entropy RL is a general exploration strategy that provides a bonus reward proportional to the entropy of the current policy. That is, $r_t^i = \lambda \mathcal{H}[\pi(\mathbf{a}_t | \mathbf{s}_t)]$. In all our experiments, we set $\lambda = 1$.

Random Agent To test a random baseline model for embodied control, we use a randomly initialized agent with the same model architecture (described in section 3, Figure 2A, and in PPO implementation details below).

Whole-brain Average We use the average recorded neural-glia activity during a specified behavioral transition in one larval zebrafish to predict whole-brain neural-glia activity recorded from another larval zebrafish undergoing the same transition. The alignment under the metric described in section 3 is computed using the average response of each cell-type (neural and glial) from the source animal to predict the corresponding cell-type in the target animal. We use two subjects and report the total alignment as the sample-weighted average between scores from both source-target pairs.

Gaussian-Process We fit a separate Gaussian Process (GP) to each cell-type (neural and glial) for each subject, using a radial basis function (RBF) kernel and centering the prior mean at the average whole-brain response. Alignment under the metric described in section 3 is computed between the whole-brain data from the target cell-type from an individual subject and its corresponding GP as the source. We use two subjects and report the total alignment as the sample-weighted average between scores from both source-target pairs.

White-noise At each timestep t , the model’s predicted next state is give by $x_{t+1} = x_t + \eta_t$, where $\eta_t \sim \mathcal{N}(0, 1)$ is white-noise. Because the metric that saturates inter-animal alignment is correlation-based, the mean and variance of this random walk are arbitrary.

PID Controller To implement the circuit-based word model proposed by Mu et al. [2] for the zebrafish brain’s transition from active to passive states, we employ a threshold-based (“bang–bang”) controller that switches the fish’s swim power $P(t)$ between an active waveform $P_{\text{base}}(t)$ and complete cessation ($P(t) = 0$) once a cumulative “futility” signal exceeds a fixed GABAergic threshold. This controller can be interpreted as the high-gain limit of a saturated PID controller.

Perceived hydrostatic drift is modeled as a constant v_d . The motor plant converts swim power into a counter-drift locomotor velocity with gain g_{MS} ,

$$v_s(t) = v_d - g_{\text{MS}}P(t).$$

Visual mismatch is the product of forward stimulus velocity and ongoing motor drive but is rectified to ignore overshoot,

$$e(t) = \begin{cases} v_s(t)P(t), & \text{if } v_s(t) > 0, \\ 0, & \text{otherwise.} \end{cases}$$

A leaky integrator with time constant τ_F accumulates the mismatch (i.e., the futility):

$$\dot{F}(t) = -\lambda_F F(t) + k_F e(t),$$

where $\lambda_F = 1/\tau_F$ and k_F is a gain. A second leaky integrator converts sustained futility into an inhibitory drive,

$$\dot{G}(t) = -\lambda_G G(t) + k_G \max(0, F(t) - \theta_F),$$

$$P(t) = \begin{cases} P_{\text{base}}(t), & G(t) \leq \theta_G, \\ 0, & G(t) > \theta_G. \end{cases}$$

To mimic experimental perturbations we set $g_{MS} = 0$ between $t_{OL\ on}$ and $t_{OL\ off}$, effectively clamping optic-flow feedback.

D Implementation Details

Proximal Policy Optimization (PPO) In all our experiments, we train our agents with PPO using a clipped surrogate objective [47] with $\epsilon^{CLIP} = 0.2$ and normalized advantage function computed using Generalized Advantage Estimation (GAE) [52] with $\lambda^{GAE} = 0.95$. The policy network is an MLP with two hidden layers [128, 64] optimized by Adam [53] with learning rate $\alpha = 0.0003$ and gradients computed over 5 epochs of 1000-step trajectories with a 250-step batch size vectorized across 64 environments. This MLP parameterizes the policy as a 5-dimensional diagonal Gaussian distribution which is sampled to produce actions during training. For evaluation (the experiments in section 4), the policy is deterministic by taking actions as the mean of the distribution. The intrinsic rewards are normalized by dividing by a running estimate of the standard deviation of the sum of discounted rewards with discount factor $\gamma = 0.99$, which then supervises the value network MLP with two hidden layers [128, 64] to estimate the expected discounted return using this same discount factor. Both policy and value networks compute on hidden states from separate LSTM blocks (Figure 2A) using a shared embedding from the sensory feature extractors. Image embeddings are obtained from 64x64 pixel observations passed through a three-layer ResNet resulting in outputs with a spatial resolution of 16x16 (closely matching the visual acuity of larval zebrafish at the final layer). Image embeddings were flattened and concatenated with proprioceptive features including joint positions and rotational velocities and their embeddings from a two-layer MLP with hidden size [64, 64].

Intrinsic Drive Module (IDM) The IDM architecture details vary depending on which intrinsic drive it implements, and is described on a case-by-case basis in the sections below. Here, we describe the commonalities between intrinsic drives, which include the optimizer, forward dynamics loss, general forward model architecture, and memory buffer parameters. Each forward dynamics model across intrinsic drives is implemented as a two-layer MLP with hidden sizes [512, 512], trained to predict the true observation one time-step into the future from the current observation using an MSE loss (where inference is done in feature-space), and optimized using Adam [53] with learning rate $\alpha = 0.001$. The IDM maintains a memory buffer of the last 100 observation embeddings from each environment in the vector and trains its constituent networks on this buffer every 20 steps. The IDM is trained for $1e^5$ steps before the intrinsic rewards are observed by the agent.

3M-Progress The ethological memory is created (with the default configuration outlined above) by training a swimmer agent on a simple navigation task in a head-free version of the experimental protocol outlined in section 3. This environment is chosen to provide the forward model with a similar visual input space as the head-fixed version while maintaining the ethology of unconstrained swimming in which the agent experiences naturalistic fluid forces and positional displacement in response to swim commands. The task is implemented as shaped reward proportional to the distance of the agent from a target location that in front of the agent, such that the swim-to-target behavior results in stabilizing the constant backwards flow of the high-contrast grating. The episode is long enough that optimizing this reward allows the agent to become passive was the target is reached. Together, our setup allows the agent to experience state-action-state triplets (current state, current action, and resulting state) associated with active and passive behaviors. This provides a close correspondence between sensory-motor coupling in our virtual ethological environment and the closed-loop experimental condition in Mu et al. [2], where larval zebrafish swim against the passive backwards flow of high-contrast gratings motivated by positional homeostasis. Although our agent is motivated to swim by a different signal than its biological twin (i.e., moving towards a target location rather than a homeostatic drive that resists displacement from an opposing current), the design of the virtual environment renders the sensory-motor stream experienced by the internal world model equivalent between scenarios, since in both cases optic flow is counteracted by forward swim motion. Because this sensory-motor stream and its resulting world-model alone define the ethological memory, the discrepancy in the signal that drove behavior has no bearing on training the new policy and value network in the open-loop environment (Figures 1D, 2B).

In the open-loop environment, the agent randomly initializes a new world-model memory that is trained online with the default configuration outlined in the IDM section. The ethological world-model memory is loaded from earliest checkpoint where the agent achieved optimal swim-to-target behavior

and its weights are frozen. The model-memory-mismatch is computed as the MSE between the predictions from each memory, filtered by an exponential moving average with timescale $\gamma = 0.99$, and the difference filtered and unfiltered predictions are passed through an L_1 activation.

Random Network Distillation (RND) [4] For RND both target and predictor networks are implemented using the default configuration in the IDM section. The predictor network is trained to predict random feature projections from the target as described in section 3.

Intrinsic Curiosity Module (ICM) [3] In addition to a forward model implemented using the default configuration in the IDM section, the ICM implements an inverse dynamics model as an MLP with an identical architecture and optimization routine to train a one-layer MLP on top of sensory features. The forward and inverse networks are cotrained by minimizing a joint objective $\beta L_F + (1 - \beta)L_I$, where L_F and L_I are the forward and inverse MSE loss functions, respectively. In our experiments, we set $\beta = 0.2$.

Disagreement [5] We use $N = 3$ randomly initialized independent forward models using the default configuration described in the IDM section. Disagreement is computed as the mean variance across feature dimensions.

γ -Progress [6] Using a randomly initialized forward model implemented using the default configuration in the IDM section, the trailing memory is created by copying these initial weights and updating them using an exponential moving average with timescale γ . In all our experiments, we use $\gamma = 0.99$.